



A model-based analysis of physiological properties of the striatal medium spiny neuron

Jing Wang, Shenquan Liu, Hongchu Wang, Niansheng Ju & Yanjun Zeng

To cite this article: Jing Wang, Shenquan Liu, Hongchu Wang, Niansheng Ju & Yanjun Zeng (2016): A model-based analysis of physiological properties of the striatal medium spiny neuron, Neurological Research

To link to this article: <http://dx.doi.org/10.1080/01616412.2015.1110304>

 View supplementary material 

 Published online: 06 Feb 2016.

 Submit your article to this journal 

 Article views: 20

 View related articles 

 View Crossmark data 

A model-based analysis of physiological properties of the striatal medium spiny neuron

Jing Wang¹, Shenquan Liu¹, Hongchu Wang², Niansheng Ju¹, Yanjun Zeng³

¹School of Mathematics, South China University of Technology, Guangzhou 510640, China, ²School of Mathematics science, South China Normal University, Guangzhou 510631, China, ³Biomedical Engineering Center, Beijing University of Technology, Beijing 100022, China

As the principal cell of the striatum, medium spiny neurons (MSNs) are closely associated with various motor dysfunctional diseases. In this paper, we describe an electric compartment model constructed in NEURON with a realistic morphology. Based on a 554-compartment computational model, we researched the influence of external current stimuli, different ions conductance, and the removal of partial dendrites on the physiological properties of the MSN. The main results are the following: (1) in the case of external current stimuli, various firing patterns appear in the MSN and the model produces a clear period-adding bifurcation phenomenon; (2) the effect of distinct types of ion channels vary and significant differences in discharge rhythm exist even among ion channels of the same type; (3) the closer the removed dendrite was to the soma, the larger the impact this had on the discharge pattern of the MSN.

Keywords: Medium spiny neuron (MSN), Discharge rhythm, Interspike intervals (ISI), The number of spikes per burst (NS)

1. Introduction

As a specialized type of inhibitory neuron, medium spiny neurons (MSNs) comprise up to 97% of the striatal interneuron population¹. Studies have demonstrated that MSNs are involved in various processes, including movement, mnemonic, and cognitive functions²⁻⁴. In addition, pathological changes in the MSN may induce a variety of cognitive and movement disorders, typically Parkinson's disease⁵, Huntington's disease⁶, and Wilson's disease⁷. MSN plays a critical role in the basal ganglia, because of its importance in receiving and integrating various input information from the cerebral cortex and thalamus⁸. Therefore, analyzing the inherent properties of MSNs and gaining insight into their role in the striatum and basal ganglia are a task both vital and urgent.

MSNs contain a variety of active channels including Na⁺ channels, K⁺ channels, and Ca²⁺ channels⁹. A salient hallmark of MSNs' behavior is the discharge pattern of the bistable membrane potential during spontaneous activity¹⁰. The bistable pattern of activity refers to rapid spontaneous transitions between two steady-state membrane potentials which are nearly 20 mV in amplitude. The bistable state has been suggested as a mechanism

for gating afferent inputs from the prefrontal cortex to nucleus accumbens, and abnormal gating could lead to the pathophysiology of schizophrenia^{10,11}. *In vivo* Wilson and Kawaguchi found the current–voltage relationship for the hyperpolarized down state showed great influence on an inwardly rectifying potassium conductance, while the depolarized up state is dominated by fast A-type (KAf), slow A-type (KAs) potassium currents during which action potential emerges¹². Moreover, Carter and Sabatini found T-type (CaT) calcium channel decreases and L-type (CaL) calcium channel increases in the up-state transition¹³.

In this paper, we study the inherent properties three aspects of the MSN by constructing a multi-compartment model which is very similar to the actual neuron. We mainly focus on the role of external current stimuli, different ion channels, and dendritic topological structure on neuronal discharge characteristics, aiming at analyzing the firing properties of the MSN.

2. Model and methods

2.1 Morphological and physiological modeling

An electric compartment model is constructed based on realistic biological anatomy experiments conducted by Spiga et al.¹⁴ The simulation files are available from the ModelDB database (<https://senselab.med.yale.edu/modeldb>, accession number 126640). The topological structure

*Correspondence to Shenquan Liu: School of Mathematics, South China University of Technology, Guangzhou 510640, China. Email: mashqliu@scut.edu.cn

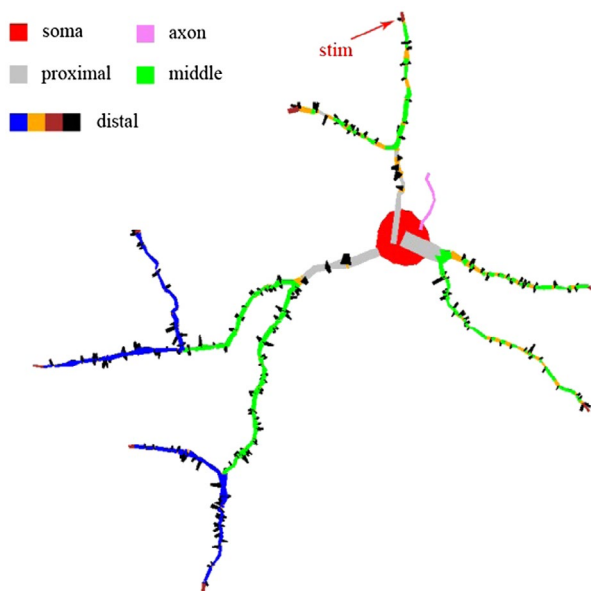


Figure 1 Morphology of a striatal medium spiny neuron composed of 554 compartments. The red arrow represents the site of stimulation.

of this model is shown in Fig. 1. The original model only contains four types of ion channels for all compartments, namely fast sodium channel (NaF), fast A-type (K_{AP}), slow A-type (K_{AS}), and four-AP resistant persistent (K_{RP}) potassium channels. Based on previous research¹⁵, we modified the original model and added 14 types of voltage-gated ion channels, namely fast (NaF) and persistent (NaP) sodium channels; fast A-type (K_{AP}), slow A-type (K_{AS}), inwardly rectifying (K_{IR}), four-AP resistant persistent (K_{RP}), large-conductance calcium-dependent (BKCa), and small-conductance calcium-dependent (SKCa) potassium channels; N-(CaN), Q-(CaQ), R-(CaR), and L-type (CaL1.2) high-voltage-activated calcium channels; T-(CaT), and L-type (CaL1.3) low-voltage-activated calcium channels. Our modified model accession number is 183994. Specific parameters for each ion channel are shown in Table 1. The variation of parameters, such as NaF, NaP, K_{AP} , K_{AS} , and K_{RP} channels, depends on the compartment location. In Table 1, the characters *s*, *a*, *p*, *m*, and *d* stand for the soma, axon, proximal, middle, and distal dendrites, respectively.

2.2 Multi-compartment model

In the theoretical analysis of the electric properties of the neuron, we adopt conductance-based Hodgkin-Huxley models to describe a single cell. According to the morphology of cell, the neuron is divided into 554 compartments (soma: 4 compartments, axon: 1 compartment, proximal dendrites: 11 compartments, middle dendrites: 103 compartments, distal dendrites: 435 compartments). The connection between different compartments is characterized by a discrete format of Rall's cable model. On the basis of previous reports^{16,17}, the current balance equation of each compartment model is represented as:

Table 1 Parameters for ionic currents

Channels: Na and K	Location	<i>g</i> (S/cm ²)
NaF	(s) (a, p, m, d)	1.5 0.195
NaP	(s) (a, p, m, d)	4e-5 1.38e-7
K_{AP}	(s) (a, m, d)	0.5 0.021
K_{AS}	(s) (a, m, d)	0.0104 9.51e-4
K_{IR}	(s, a, p, m, d)	1.4e-4
K_{RP}	(s)	0.001
BKCa	(s, a, p, m, d)	0.001
SKCa	(s, a, p, m, d)	0.145
Channel: Ca	Location	<i>p</i> (cm/s)
CaL1.2	(s, a, p, m, d)	6.7e-6
CaL1.3	(s, a, p, m, d)	4.25e-7
CaN	(s, a, p, m, d)	1e-5
CaQ	(s, a, p, m, d)	6e-6
CaR	(s, a, p, m, d)	2.6e-5
CaT	(s, a, p, m, d)	4e-7

$$C \frac{dV_i}{dt} = -I_{ion} + I(t) + \frac{V_{i-1} - V_i}{R_{i-1,i}} - \frac{V_i - V_{i+1}}{R_{i,i+1}}. \quad (1)$$

Here, *C* denotes the cell membrane capacitance and V_i is the membrane potential of the *i*th compartment. I_{ion} represents ionic currents of the *i*th compartment. $I(t)$ represents the current induced by external stimuli. The compartment interchange currents connected by connection strength $R_{i-1,i}$ and $R_{i,i+1}$ are described by the last two terms in Eq. (1). The voltage-dependent gating variables are represented as:

$$\frac{dx}{dt} = \frac{x_{\infty}(V) - x}{\tau_x}. \quad (2)$$

In Eq. (2), $x = x(V)$ stands for the open status of different ion channels; $x_{\infty}(V)$ represents the steady-state values of gating variables and τ is the activation time constant.

Numerical simulations of the multi-compartment medium spiny neuron were modeled using NEURON software¹⁸ and run with a variable time step. In addition, we processed the data and images by means of Python software. The simulation results have been repeatedly verified. In this paper, all action potentials refer to the somatic membrane potentials of the MSN.

3. Stimulation results and analysis

3.1 Response to external current stimuli

Studies have shown that the neuron's behavior will change as the external current is injected¹⁹. As the stimulating current is increased, the cell changes from quiescent to periodic firing and then to bursting. Therefore, we research the effect of external current stimuli on discharge rhythms of MSNs in this section. Firstly, we stimulated the soma by depolarizing and hyperpolarizing direct currents (Fig. 2a), and we found the model could reproduce firing dimorphism which has been observed *in vitro* in response to current injections by Moyer et al.²⁰. As the MSN is responsible for the relay work of the entire basal ganglia, its dendrites receive and process various input information from distinct areas, including the dopaminergic and

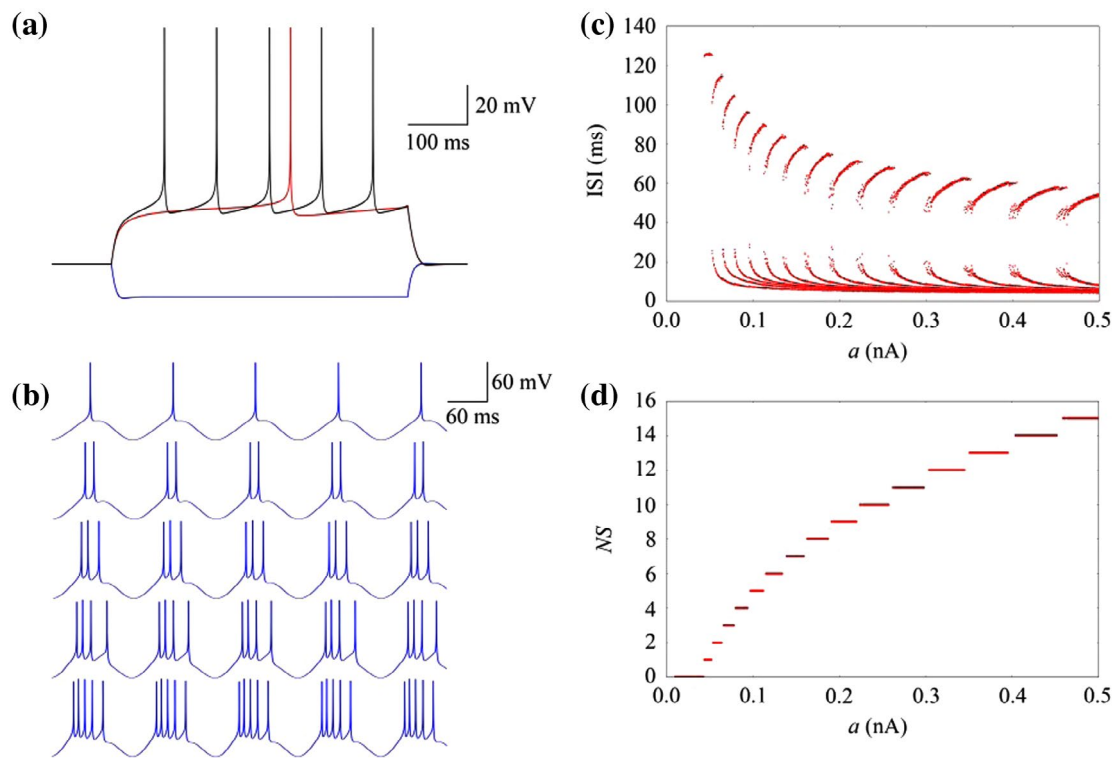


Figure 2 The medium spiny neuron's responses to external current stimuli. (a) Somatic voltage responses to depolarizing and hyperpolarizing injected currents (blue: -0.07 nA, red: 0.0688 nA, black: 0.074 nA). (b) Firing patterns of the MSN under stimulation of $I(t) = a \times (1 + \cos(0.05t))$ nA on the distal dendrite as indicated in figure 1. From top to bottom, the value of a is 0.05 , 0.06 , 0.07 , 0.08 , and 0.1 nA, respectively. (c) The interspike intervals (ISI) with respect to the stimulus intensity. (d) The number of spikes per burst (NS) with respect to the stimulus intensity.

cortical input from the mid-brain. We let the external current stimulus act on the distal dendrite, as the red arrow showed in Fig. 1. Unless otherwise stated, the position of stimulation refers to this distal dendrite, and the mode of stimulation is $I(t) = a \times (1 + \cos(\omega t))$ nA.

Fixing $\omega = 0.05$ Hz, we found that variations in stimulus intensity a will induce the change of firing patterns. From Fig. 2b, we can see, as the stimulus intensity slowly increases from 0.05 to 0.1 nA, the firing sequences of the MSN undergo very significant changes: (1) the number of spikes in each burst increases gradually; (2) the discharge patterns transit from period-1 firing to bursting. In Fig. 2c, the interspike intervals (ISI) bifurcation diagram is plotted with the linear change of a , from which we can better observe the transitions between different discharge patterns. For $a \in [0.044, 0.053]$ nA, the neuron exhibits continuous periodic spiking. As the value of a is increased, the spiking state goes through a period-adding cascade. With further increase of a , regular bursting alternates with chaotic bursting. To be intuitive, we computed the number of spikes per burst (NS) with respect to a in Fig. 2d. As can be observed below, NS presents a trapezoidal growth with the increasing of a .

Next, we attempted to research the combined influence of the stimulus frequency and intensity on neuronal discharge patterns. The diagram below with two parameters was plotted to demonstrate the neuronal firing regions

of quiescent, regular spiking, regular bursting, and chaotic bursting under different combinations of ω and a in Fig. 3. The color-scale bar on the right in Fig. 3a indicates NS running from 0 (quiescent) to 16 (chaotic bursting). Additionally, the color denoted by the number 1 in the bar to the right hand of Fig. 3a represents regular spiking and numbers 2–15 represent regular bursting. We select four representative firing modes labeled b_1 – b_4 in Fig. 3a and the corresponding membrane potential traces of these four cases are shown in Figs. 3b₁–3b₄. Model results shown in Fig. 3a illustrate that bursting is more inclined to occur when a is large, and too small a value of a will cause the neuron to become quiescent. For a given ω , the increase of a may result in a transition of discharge patterns from quiescent to spiking or from spiking to bursting. While for a given a , the increase of ω may result in no change in discharge mode or give rise to an inverse period-adding bifurcation phenomenon. By plotting the diagram of (ω, a) -biparameter, we get a further understanding of the different roles of stimulus frequency and intensity on neuronal discharge rhythms.

3.2 Effect of ion channels on somatic discharge rhythms

It has been well documented that numerous intrinsic ion channels of the MSN have a very important impact on their discharge rhythms. For example, studies have shown that

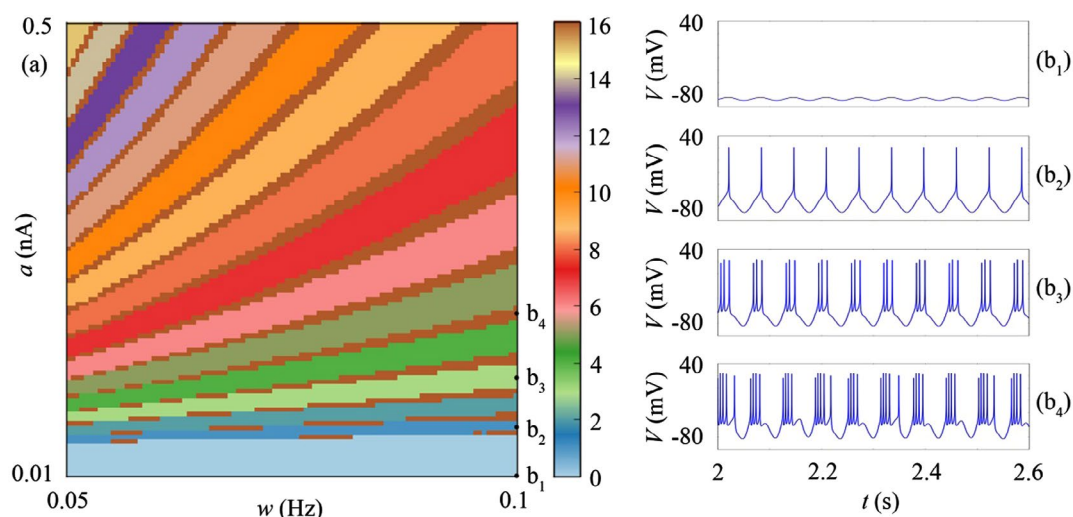


Figure 3 The number of spikes per burst (NS) is plotted as functions of the current stimulus intensity and angular frequency, associating different color codes to different NS . (a) (w, a)-biparametric screening plane demonstrates the stages of the spike-adding cascade and picks out regions of chaotic bursting. The color bar on the right gives NS scaling from 0 to 16. The number 0 denotes the resting state, in which the neuron does not produce action potentials. The number 1 stands for regular spiking. Numbers 2–15 represent regular bursting, and chaotic bursting is scattered throughout as brown dots, a color corresponding to the number 16 in the bar to the right of Fig. 3a. (b₁)–(b₄) Examples of quiescent, regular spiking, regular bursting, and chaotic bursting. From top to bottom, the value of (w, a) is (0.1, 0.01), (0.1, 0.06), (0.1, 0.11), and (0.1, 0.18), respectively.

Na channels have a close relationship with Parkinson's disease²¹; K channels are correlated with a wide variety of physiological activities^{22,23}; Ca channels blocker may hold the key to a potential treatment for Huntington's disease²⁴. Therefore, the analysis of various ion channels is essential. Herein, we mainly analyze the role of the maximum conductivity coefficient of ion channels on somatic discharge rhythms. The form of external current stimuli $I(t) = 0.1 \times (1 + \cos(0.05t))$ is the same as in the previous study, which is still acting on the distal dendrite.

3.2.1 The role of sodium channels

The multi-compartment model contains two sodium channels; namely fast and persistent sodium channels. Here, we chose the maximum conductivity coefficient of the somatic fast sodium channel (g_{NaF}) to analyze it. Fig. 4 shows one-dimensional bifurcation diagrams for the model with g_{NaF} as the control parameter. In Fig. 4a, along with the increase of g_{NaF} , firing patterns transit from chaotic bursting (when $g_{NaF} = 1$ S/cm²) to period-5 bursting (when $g_{NaF} = 2$ S/cm²). With further increase of g_{NaF} , a period-6 pattern develops via a chaotic region ($g_{NaF} \in [3, 4.14]$ S/cm²). In Fig. 4b, as g_{NaF} increases from 1 S/cm² to 5 S/cm², neuronal maximum action potentials increase from about 3 to 45 mV. Specific details are shown in Fig. 4c. Actually, as well as neuronal maximum action potentials significantly increase, minimum action potentials slightly decrease.

The above analysis shows that small changes in g_{NaF} have a significant effect on neuronal activities or action potentials, demonstrating that the main role of fast sodium

channel is to depolarize and excite the neuron rapidly generating action potentials.

3.2.2 The role of potassium channels

In the model, there are six types of potassium channels. Here, we analyze the fast and slow A-type potassium channels. Previous studies have shown that A-type potassium currents are the primary determinant of regulating spontaneous, low-frequency, and repetitive firing^{25,26}. ISI bifurcation diagrams with respect to g_{KAf} and g_{KAs} are presented in Fig. 5a and 5b, respectively. With the decrease of g_{KAf} and g_{KAs} , neuronal firing patterns transit from period-1 spiking (when $g_{KAf} = 1.8$ S/cm² or $g_{KAs} = 0.008$ S/cm²) to bursting, and the corresponding ISI bifurcation diagram exhibits a period-adding bifurcation phenomenon. Furthermore, with the increase of g_{KAf} , neuronal maximum action potentials approximate linear decrease from 22.5 to 3 mV (as shown in Fig. 5c). It is worth noting that this phenomenon is completely opposite to the influence of g_{NaF} . From here, we may draw a conclusion that the effect of fast A-type potassium channel on neuronal depolarization is contrary to that of persistent sodium channel.

3.2.3 The role of calcium channels

For calcium channels, we select the N-type high-voltage-activated calcium channel to analyze it. As can be seen from ISI sequences (Fig. 6a), with the increase of p_{CaN} from 0 to 0.00022 cm/s, the model exhibits an inverse period-adding bifurcation scenario. Then a period-5 pattern develops via a narrow chaotic region. When p_{CaN} is in the range of 0.000268 cm/s to 0.000666 cm/s, the model

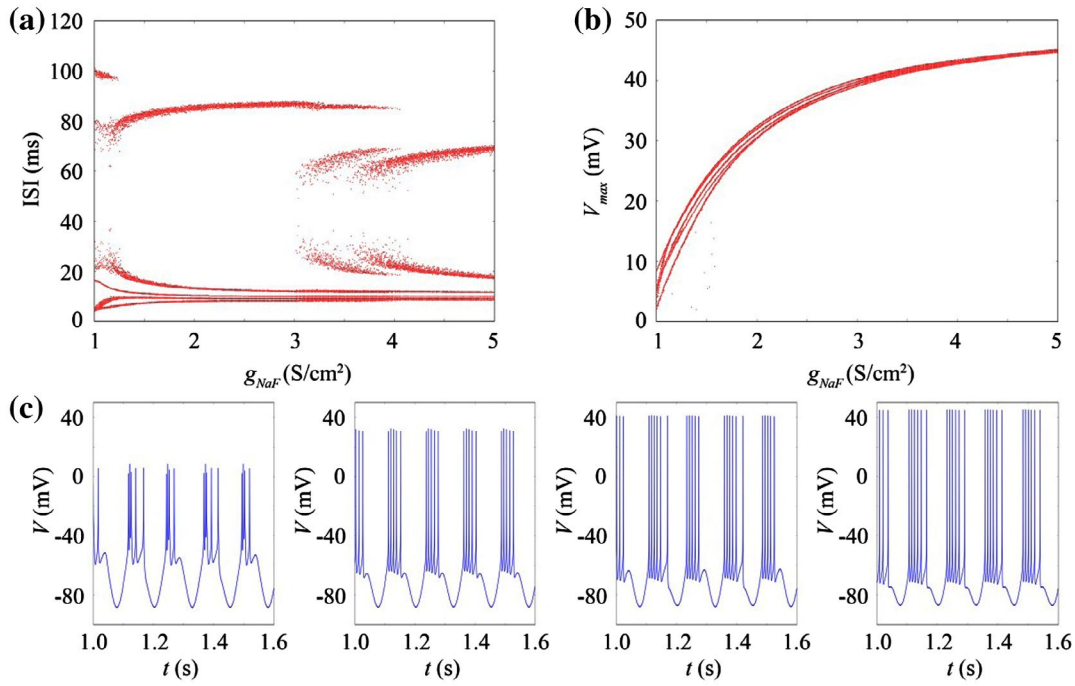


Figure 4 Bifurcation diagrams of interspike intervals and maximum action potentials with variations of g_{NaF} . (a) Interspike intervals. (b) Maximum action potentials. (c) Firing patterns with the variation of g_{NaF} . From left to right, the value of g_{NaF} is 1, 2, 3.3, and 5 S/cm², respectively.

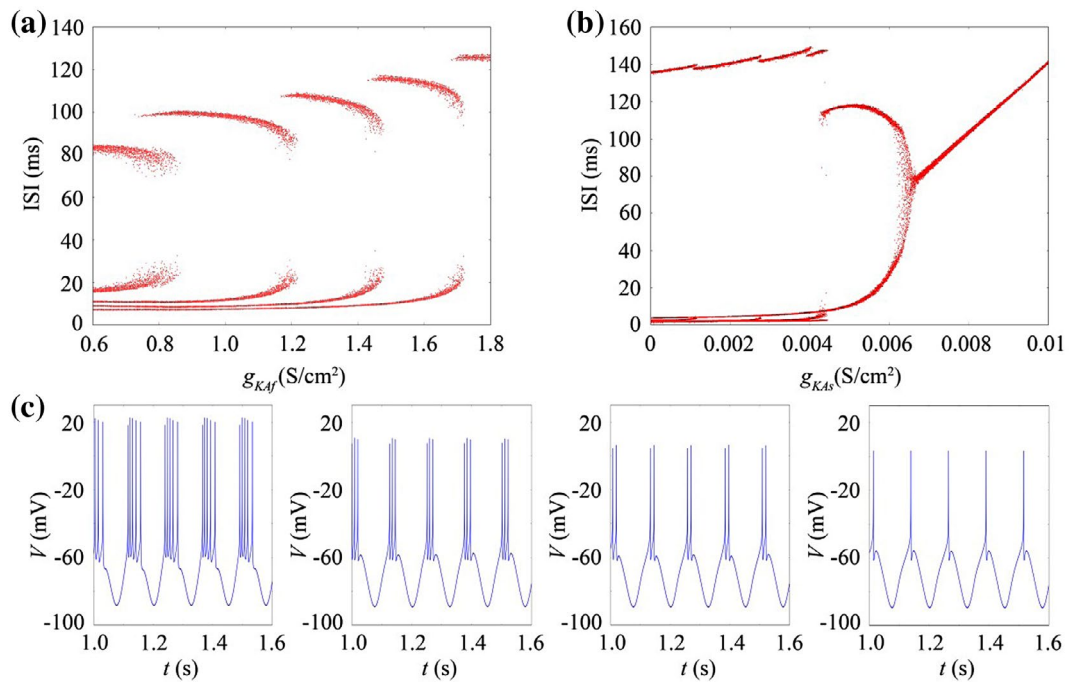


Figure 5 Bifurcation diagrams of interspike intervals. (a) Interspike intervals with respect to g_{KAF} . (b) Interspike intervals with respect to g_{KAs} . (c) Firing patterns with the variation of g_{KAF} . From left to right, the value of g_{KAF} is 0.6, 1.3, 1.6, and 1.8 S/cm², respectively.

is in a period-2 bursting. With further increase of p_{CaN} , the model enters into another chaotic region. Hereafter, periodic bursting patterns emerge. For $p_{CaN} \geq 0.000928$ cm/s, the model presents continuous periodic spiking. These transitions between different firing patterns can also be observed in Fig. 6b.

Through the above analysis, we can draw that small changes in p_{CaN} have a significant influence on neuronal

activities, specifically embodied in transitions between different firing patterns and variations in discharge intensity (the number of spikes per burst).

3.3 The variations of dendritic topological structure

The medium spiny neuron projects the unique structure of dendrites which can receive information input from different

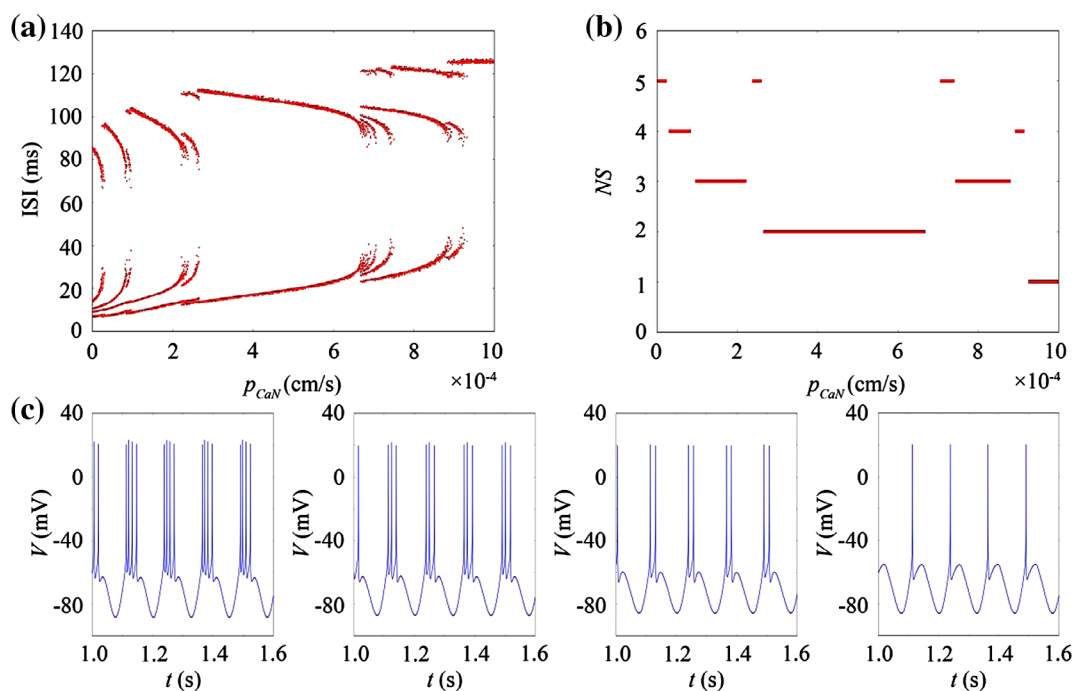


Figure 6 Bifurcation diagrams of interspike intervals and the number of spikes per burst (NS). (a) Interspike intervals with respect to p_{CaV} . (b) The number of spikes per burst with respect to p_{CaV} . (c) Firing patterns with the variation of p_{CaV} . From left to right, the value of p_{CaV} is 0.00005, 0.00015, 0.0004, and 0.001 cm/s, respectively.

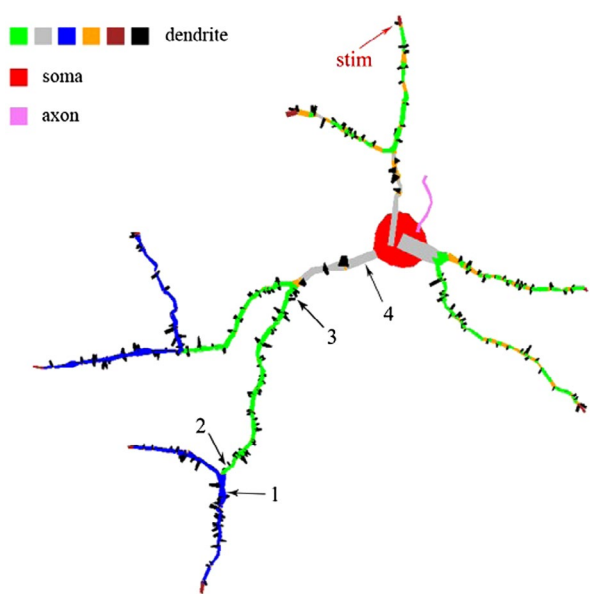


Figure 7 The removal positions of dendrites. Marked black arrows in the figure represent corresponding removal positions 1, 2, 3, and 4. The red arrow represents the site of stimulation.

regions to all directions. What's more, these dendritic topological structures play an important role in receiving and processing the afferent information. Moreover, biological experiments have proved that Huntington's disease is a neurodegenerative disease caused by degradation and death of the MSN⁶. Based on the above factors, we analyze the variations of dendritic topological structure on neuronal discharge process, by utilizing the method of removing part dendrites to imitate the degradation and death process. External current

stimulation used here has the same pattern and magnitude as before, and the stimulating position remains unchanged. In Fig. 7, the red arrow represents the site of stimulation. For comparative analysis, we select four different removal positions indicated by black arrows, relative to soma from far to near.

In the following, we research neuronal activities of the full neuron and the corresponding four removal positions. First, different discharge sequences of the MSN are analyzed. From Fig. 8, we can see the somatic firing patterns still present periodic bursting when part of dendrite is removed. The number of bursts in the same time has no apparent change, but the number of spikes in a burst significantly reduces with the removal position relative to soma from near to far. Furthermore, the farther away from soma the removal position is, the closer discharge pattern is to the full neuron.

Next, we compare the amplitude of discharge sequences in Fig. 8. As shown in Fig. 9a, the mean maximum value of membrane potentials (V_{max}) obviously increases with the increase of removal parts. When the removal position is far away from soma, V_{max} slightly increase. However, for the removal position near soma, V_{max} increases faster, which can be seen from the slope of each segment in Fig. 9a. In other words, the nearer the removal part of the soma, the greater impact of neuronal membrane potentials the MSN is subject to. Moreover, we consider the mean firing rate (MFR) and the mean lasting time (MLT) in Fig. 9b and 9d, respectively. At the removal position 1 and 2, MFR remains unchanged, but MLT gradually decreases. For more recent removal position 3 and 4, both MFR and MLT have a sharp increase.

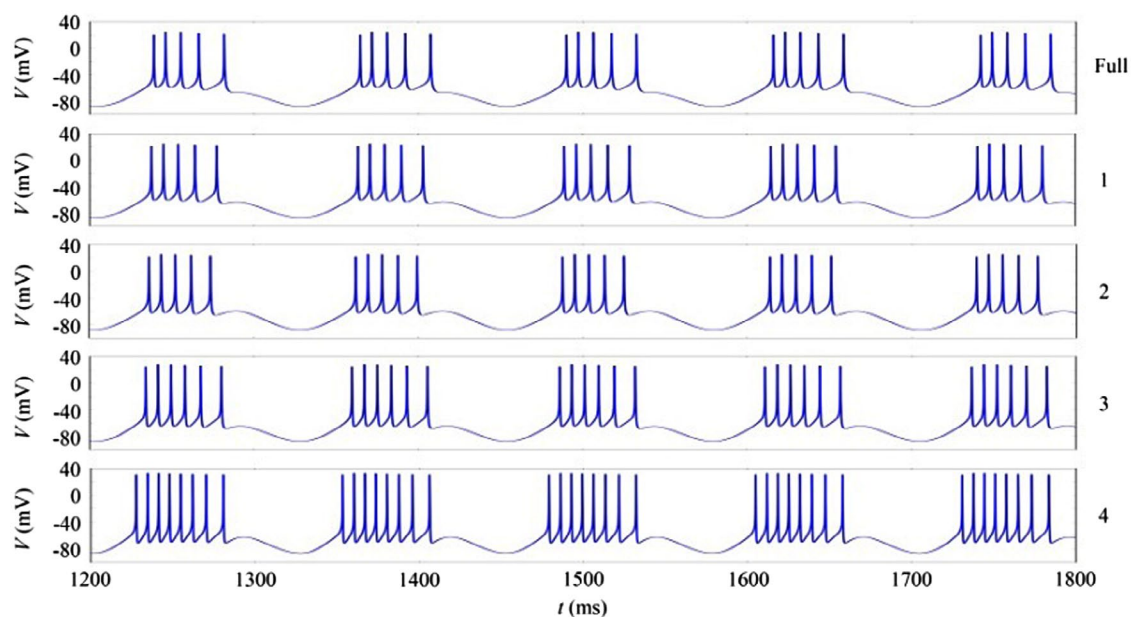


Figure 8 Time series of the membrane potential. From top to bottom, the diagrams separately represent the full neuron, the corresponding removal positions 1, 2, 3, and 4 in figure 7.

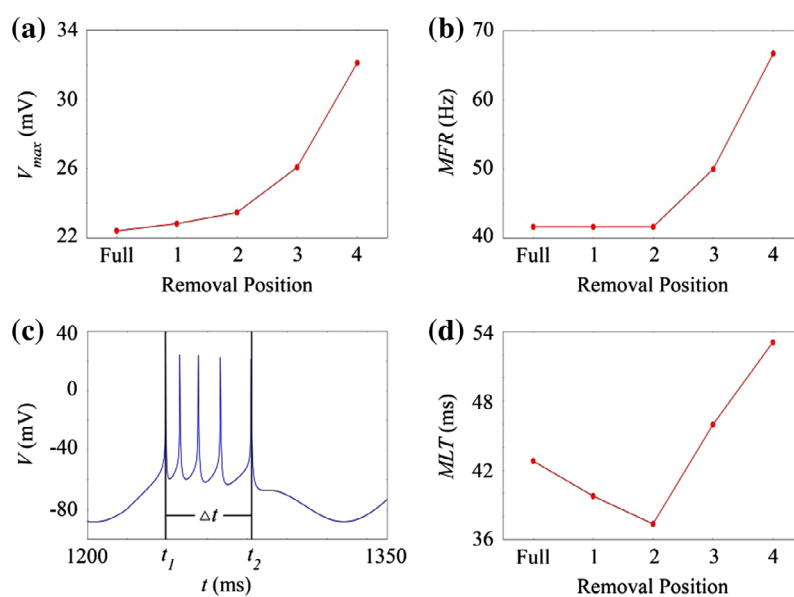


Figure 9 Dynamical phenomena of the MSN with the removal positions of dendrites. (a) The mean maximum value of membrane potentials (V_{max}) with respect to the removal position. (b) The mean firing rate (MFR) with respect to the removal position. (c) Lasting time $\Delta t = t_2 - t_1$, where t_1 and t_2 separately indicate the time of arrived peak and spiking lasting. (d) The mean lasting time (MLT) with respect to the removal position.

From the above analysis, we can find that the integrity of the dendritic topological structure of the MSN has a great influence on its neuronal activities. In particular, the discharge intensity and amplitude significantly change. In addition, the removal part near from soma has a more remarkable influence on neuronal activities than that far away from soma.

4. Discussion

In this paper, we research a multi-compartment model of the medium spiny neuron based on real morphological data. Inspired by the research of Steephen and Manchanda¹⁵, we

add 14 types of ion channels so that the model could reproduce the electrophysiological properties of the neuron. We investigate its abundant discharge characteristics by changing external current stimuli, parameters of internal ion channels, and dendritic structure. According to the numerical simulation results, we find both internal factors and external factors have a major impact on the firing rhythm of the MSN. Our major observations are summarized as follows:

1. For direct current stimulus, the model reproduces well-firing dimorphism; for mixed current stimulus, both stimulus intensity and frequency have a significant influence on discharge rhythms, showing transitions from spiking to bursting and transitions between distinct bursting patterns.

This suggests that the neuron handles different input information in different ways.

- By comparing the variations of the maximum conductivity coefficient of somatic sodium, potassium, and calcium channels, we conclude that (1) the effect of different types of ion channels is different; (2) the same type of ion channels has a distinct effect on neuronal discharge rhythms. This indicates that subtle changes of neuronal intrinsic biological properties have a significant impact on the mode of encoded information.
- The influence of changes in dendritic topological structure of the MSN on neuronal activities demonstrates that (1) the partial degradation of dendrite affects its discharge rhythm; (2) the morphological mutation which is near soma generates greater impact, and even affects the ability of neurons to encode information. It provides a good idea to deeply understand the reason of Huntington's disease caused by degradation and death of the MSN.

In the previous research, the influence of inactivating inward rectifying potassium current (inK_{IR}) was analyzed by building computational models of MSNs with and without inK_{IR} ¹⁵. The researchers found inK_{IR} contributed to depolarizing and firing onset in MSNs. For the net effects of dopaminergic modulations, Moyer et al.²⁰ separately simulated D1- and D2-receptor modulation of intrinsic and synaptic currents. They found that dopaminergic modulation could lead to changes in neuronal excitability and the integration time window. As in this research, we choose three kinds of ion channels to explore the firing properties of a single neuron. Model results illustrate the effect of internal factors on the variation of firing rhythm and their corresponding bifurcation phenomena.

With the method of encoding information, neurons transfer messages to its lower neurons through the axon. The efferent information includes multiple messages, such as the space position of receiving stimulus, the stimulus intensity, and frequency. However, it is not clear for the operation mechanism of neural coding so far. We can only distinguish different mechanisms of neural coding depending on distinct neuronal discharge rhythms. Due to the limitations of biological experiment, it becomes increasingly important to imitate neurons or neural networks by means of modeling. Furthermore, with the continuous development of neuroscience and computer technology, the research on causes and laws of changes in neuronal discharge rhythms through numerical simulation draws more and more attention.

Supplemental data

Supplemental data for this article can be accessed here. [<http://10.1080/01616412.2015.1110304>]

Funding

This work was supported by the National Natural Science Foundation of China under [grant number 11172103].

References

1 Shepherd G, Grillner S, editors. Handbook of brain microcircuits. Oxford University Press, New York; 2010.

- Hikosaka O, Takikawa Y, Kawagoe R. Role of the basal ganglia in the control of purposive saccadic eye movements. *Physiol. Rev.* 2000;80:953–78.
- Voytek B, Knight RT. Prefrontal cortex and basal ganglia contributions to visual working memory. *Proc. Natl. Acad. Sci.* 2010;107:18167–72.
- Mahon S, Vautrelle N, Pezard L, Slaght SJ, Deniau JM, Chouvet G, et al. Distinct patterns of striatal medium spiny neuron activity during the natural sleep-wake cycle. *J. Neurosci.* 2006;26(48):12587–95.
- Blandini F, Nappi G, Tassorelli C, Martignoni E. Functional changes of the basal ganglia circuitry in Parkinson's disease. *Prog. Neurobiol.* 2000;62:63–88.
- Ehrlich ME. Huntington's disease and the striatal medium spiny neuron: cell-autonomous and non-cell-autonomous mechanisms of disease. *Neurotherapeutics.* 2012;9:270–84.
- Jayasundar R, Sahani AK, Gaikwad S, Singh S, Behari M. Proton MR spectroscopy of basal ganglia in Wilson's disease: case report and review of literature. *Magn. Reson. Imaging.* 2002;20:131–35.
- Doig NM, Moss J, Bolam JP. Cortical and thalamic innervation of direct and indirect pathway medium-sized spiny neurons in mouse striatum. *J. Neurosci.* 2010;30:14610–18.
- Wolf JA, Moyer JT, Lazarewicz MT, Contreras D, Benoit-Marand M, O'Donnell P, et al. NMDA/AMPA ratio impacts state transitions and entrainment to oscillations in a computational model of the nucleus accumbens medium spiny projection neuron. *J. Neurosci.* 2005;25:9080–95.
- O'Donnell P, Grace AA. Synaptic interactions among excitatory afferents to nucleus accumbens neurons: Hippocampal gating of prefrontal cortical input. *J. Neurosci.* 1995;15:3622–39.
- Grace AA. Gating of information flow within the limbic system and the pathophysiology of schizophrenia. *Brain Res. Rev.* 2000;31:330–41.
- Wilson CJ, Kawaguchi Y. The origins of two-state spontaneous membrane potential fluctuations of neostriatal spiny neurons. *J. Neurosci.* 1996;16:2397–410.
- Carter AG, Sabatini BL. State-dependent calcium signaling in dendritic spines of striatal medium spiny neurons. *Neuron.* 2004;44:483–93.
- Spiga S, Lintas A, Migliore M, Diana M. Altered architecture and functional consequences of the mesolimbic dopamine system in cannabis dependence. *Addict. Biol.* 2010;15:266–76.
- Steephen JE, Manchanda R. Differences in biophysical properties of nucleus accumbens medium spiny neurons emerging from inactivation of inward rectifying potassium currents. *J. Comput. Neurosci.* 2009;27:453–70.
- Nakano T, Yoshimoto J, Doya K. A model-based prediction of the calcium responses in the striatal synaptic spines depending on the timing of cortical and dopaminergic inputs and post-synaptic spikes. *Front. Comput. Neurosci.* 2013;7:119.
- Migliore M, Shepherd GM. Dendritic action potentials connect distributed dendrodendritic microcircuits. *J. Comput. Neurosci.* 2008;24: 207–21.
- Carnevale NT, Hines ML, editor. The NEURON book. Cambridge University Press, New York; 2006.
- Laing CR, Longtin A. Periodic forcing of a model sensory neuron. *Phys. Rev. E.* 2003;67:051928.
- Moyer JT, Wolf JA, Finkel LH. Effects of dopaminergic modulation on the integrative properties of the ventral striatal medium spiny neuron. *J. Neurophysiol.* 2007;98:3731–48.
- Maurice N, Mercer J, Chan CS, Hernandez-Lopez S, Held J, Tkatch T, et al. D2 dopamine receptor-mediated modulation of voltage-dependent Na^+ channels reduces autonomous activity in striatal cholinergic interneurons. *J. Neurosci.* 2004;24:10289–301.
- Mermelstein PG, Song WJ, Tkatch T, Yan Z, Surmeier DJ. Inwardly rectifying potassium (IRK) currents are correlated with IRK subunit expression in rat nucleus accumbens medium spiny neurons. *J. Neurosci.* 1998;18:6650–61.
- Shen W, Hernandez-Lopez S, Tkatch T, Held JE, Surmeier DJ. Kv1.2-containing K^+ channels regulate subthreshold excitability of striatal medium spiny neurons. *J. Neurophysiol.* 2004;91:1337–49.
- Tang TS, Slow E, Lupu V, Stavrovskaya IG, Sugimori M, Llinas R, et al. Disturbed Ca^{2+} signaling and apoptosis of medium spiny neurons in Huntington's disease. *Proc. Natl. Acad. Sci. U. S. A.* 2005;102:2602–07.
- Song WJ, Tkatch T, Baranauskas G, Ichinohe N, Kitai ST, Surmeier DJ. Somatodendritic depolarization-activated potassium currents in rat neostriatal cholinergic interneurons are predominantly of the A type and attributable to coexpression of Kv4.2 and Kv4.1 subunits. *J. Neurosci.* 1998;18:3124–37.
- Tkatch T, Baranauskas G, Surmeier DJ. Kv4.2 mRNA abundance and A-type K^+ current amplitude are linearly related in basal ganglia and basal forebrain neurons. *J. Neurosci.* 2000;20:579–88.